

Reliability of merger tree realizations of dark halos in the Monte-Carlo modeling of galaxy formation

Mamoru SHIMIZU,¹ Tetsu KITAYAMA,² Shin SASAKI³ and Yasushi SUTO^{1,4}

¹Department of Physics, School of Science, The University of Tokyo, Tokyo 113-0033

mshimizu@utap.phys.s.u-tokyo.ac.jp

²Department of Physics, Toho University, Funabashi, Chiba 274-8510

³Department of Physics, Tokyo Metropolitan University, Hachioji, Tokyo 192-0397

⁴Research Center for the Early Universe, School of Science, The University of Tokyo, Tokyo 113-0033

(Received 2001 November 29; accepted 2002 July 11)

Abstract

We examine the reliability of the merger trees generated for the Monte-Carlo modeling of galaxy formation. In particular we focus on the cold gas fraction predicted from the merger trees with different assumptions on the progenitor distribution function, the timestep, and the mass resolution. We show that the cold gas fraction is sensitive to the accuracy of the merger trees at small-mass scales of progenitors at high redshifts. One can reproduce the Press-Schechter prediction to a reasonable degree by adopting a fairly large number of redshift bins, $N_{\text{step}} \sim 1000$ in generating merger trees, which is a factor of ten larger than the canonical value used in previous literature.

Key words: cosmology: theory - galaxies: formation - galaxies: halos

1. Introduction

Understanding formation and evolution of galaxies is a fundamental step in linking the initial condition of the universe and the cosmological observational data. Recent systematic studies of high-redshift objects such as quasars and Lyman-break galaxies should provide important clues to the early universe although their proper interpretation is often not so straightforward mainly because those objects certainly do evolve in time.

A theoretical study of galaxy evolution, especially its spectroscopic evolution, in cosmological context was begun by Tinsley (1980) and followed by many authors (e.g., Bruzual 1983; Arimoto, Yoshii 1986; Guiderdoni, Rocca-Volmerange 1987; Charlot, Bruzual 1991; Bruzual, Charlot 1993; Kodama, Arimoto 1997). These studies are based on a so-called ‘one-zone’ model which assumes that a galaxy does not interact with other galaxies. It is fairly established now, however, that structures in the universe have built up hierarchically from small to large scales as in a cold dark matter (CDM) model. This means that a galaxy interacts and sometimes merges with other galaxies even if it was an isolated system at birth. The predictions in the one-zone model therefore may be significantly different from what happened to galaxies in a hierarchical universe.

White & Frenk (1991) developed a detailed analytic formalism to describe formation and evolution of galaxies taking account of the hierarchical merging of dark matter halos, gas cooling, star formation and supernova feedback. Subsequent numerical approaches in modeling hierarchical merging of dark halos employ two somewhat different algorithms; one is called the ‘block model’ in which a random-Gaussian density fluctuation field is generated by

dividing a hypothetical rectangular box recursively (Cole, Kaiser 1988; Cole 1991; Cole et al. 1994). While this algorithm is simple and straightforward, the resulting halo masses are necessarily binned in discrete steps of a factor of two. The other generates a realization of halo merger trees according to a probability distribution function predicted by the extended Press-Schechter theory (Bower 1991; Bond et al. 1991; Kauffmann, White 1993; Somerville, Kolatt 1999; Sheth, Lemson 1999). The latter is widely used in studying the cosmological evolution of galaxies in a hierarchical universe (Kauffmann et al. 1993; Baugh et al. 1998; Somerville, Primack 1999; Cole et al. 2000; Nagashima, Gouda 2001). Throughout the present paper, we call the latter method the Monte-Carlo modeling of merger histories (simply, the Monte-Carlo modeling) while it is usually referred to as a semi-analytic model of galaxy formation (SAM).

The most important ingredient in the Monte-Carlo modeling is the conditional joint-probability distribution function of a set of *progenitor* halos of mass M_2^j at a redshift z_2 which is a part of a *parent* halo of mass M_1 at z_1 , conceptually written as

$$\text{Prob}(M_2^1, M_2^2, \dots, M_2^N, z_2 | M_1, z_1) dM_2^1 dM_2^2 \dots dM_2^N \quad (N = 1, \dots, \infty). \quad (1)$$

Unfortunately only an analytical expression for the conditional one-point probability distribution function, $\text{Prob}(M_2^i, z_2 | M_1, z_1)$, is known on the basis of the extended Press-Schechter theory (for the special case of the Poisson initial power spectra, see a different approach by Sheth, Lemson 1999), and thus one needs to employ an additional *assumption* in generating realizations of merger trees of halos in general (e.g., Kauffmann, White 1993; Somerville, Kolatt 1999). Furthermore any numerical

procedure to generate them necessarily involves several *ad hoc* parameters due to the limitation of the available computation resources including the finite timestep of computation, the minimum mass of halos to be included in merger trees, and the maximum number of progenitors for each halo at each step.

The purpose of the paper is to perform a systematic investigation of possible artificial effects of the above problems on merger tree realizations, and to re-examine the validity of the Monte-Carlo modeling. In particular we focus on the extent to which the resulting merger trees reproduce the conditional one-point probability distribution function predicted by the extended Press-Schechter theory which directly changes the fraction of cold gas. Exactly for this reason, we adopt a conventional Λ CDM model with the cosmological parameters $\Omega_0 = 0.3$, $\lambda_0 = 0.7$, $h = 0.7$, $\sigma_8 = 1.0$, and $\Omega_B = 0.015h^{-2}$ (e.g., Kitayama, Suto 1997; Kitayama et al. 1998), and neglect star formation and feedback effect for definiteness.

2. Merger trees of dark matter halos

2.1. Constructing merger trees of dark matter halos

Our model of merging histories of dark matter halos is mainly based on that of Somerville, Kolatt (1999), which we adopt as our fiducial choice and slightly modify their original scheme as follows. We begin with a halo of mass $M_1 = M_{\text{root}}$ at redshift $z_1 = z_{\text{min}}$, and consider its progenitors at a slightly earlier redshift $z_2 = z_1 + \Delta z(z_1)$. Since the joint conditional probability for the progenitors (eq.[1]) is not known, we choose the i -th progenitor halo of mass M_2^i according to the *one-point* conditional probability, $\text{Prob}(M_2^i, z_2 | M_1, z_1)$, as long as $M_2^i > M_{\text{res}}$ and the total mass satisfies

$$\sum_{i=1}^N M_2^i < M_1 - \Delta M_{\text{acc}} (< M_{\text{res}}), \quad (2)$$

where

$$\Delta M_{\text{acc}} (< M_{\text{res}}) = \int_0^{M_{\text{res}}} dM_2 M_2 \frac{dN}{dM_2} (M_2, z_2 | M_1, z_1) \quad (3)$$

is the expectation value of the total mass of halos smaller than the resolution mass M_{res} with $dN/dM_2(M_2, z_2 | M_1, z_1)$ being the appropriate conditional mass function (eq.[5] below). In other words, we distinguish the discrete merging and the continual accretion at the mass M_{res} , and do not resolve the halos below M_{res} in our merger trees. Once all relevant progenitor halos are selected, we repeat the above procedure recursively for each progenitor until the maximum redshift z_{max} . Unless otherwise stated, we set $z_{\text{min}} = 0$ and $z_{\text{max}} = 15$ in the present paper. For convenience, we list in Table 1 variables which are extensively discussed in the present paper.

In the original method by Somerville, Kolatt (1999), one stops selecting progenitors when $M_1 - \sum_{i=1}^N M_2^i$ becomes less than M_{res} but without imposing the condition $M_2^i > M_{\text{res}}$. They carefully tuned the timesteps depending on M_1 so that the resulting progenitor mass function be-

comes close to equation (5) below. Rather we stop choosing the progenitor when $M_1 - \Delta M_{\text{acc}} (< M_{\text{res}}) - \sum_{i=1}^N M_2^i$ becomes negative, and the last selected progenitor M_2^N is not included in the tree. In this case, the remaining mass $M_1 - \Delta M_{\text{acc}} (< M_{\text{res}}) - \sum_{i=1}^{N-1} M_2^i$ is not necessarily smaller than M_{res} . We find that our method reproduces equation (5) even with the M_1 -independent timesteps.

2.2. Conditional probability distribution function

The most important and subtle issue is the proper choice of the *one-point* conditional probability, $\text{Prob}(M_2, z_2 | M_1, z_1)$. Bower (1991) and Bond et al. (1991) derived the conditional probability of M_2 at z_2 which is a part of halo M_1 at z_1 :

$$\frac{dP}{dM_2} (M_2, z_2 | M_1, z_1) = \frac{\delta_{c,2} - \delta_{c,1}}{\sqrt{2\pi(S_2 - S_1)^3}} \exp\left(-\frac{(\delta_{c,2} - \delta_{c,1})^2}{2(S_2 - S_1)}\right) \left| \frac{dS_2}{dM_2} \right|, \quad (4)$$

where $\delta_{c,i} \sim 3(12\pi)^{2/3}/20D(z_i)$ (its useful approximate formula may be found in Kitayama, Suto 1996) is the critical over-density of mass density field at redshift z_i , $D(z_i)$ is the linear growth rate, $S_i \equiv \sigma^2(M_i)$ is a mass variance of density field top-hat smoothed over the mass scale M_i . Since equation (4) is the *mass-weighted* probability for M_2 , it is easily translated to the *number-weighted* probability that we need in the halo number counting:

$$\frac{dN}{dM_2} (M_2, z_2 | M_1, z_1) = \frac{M_1}{M_2} \frac{dP}{dM_2} (M_2, z_2 | M_1, z_1). \quad (5)$$

Figures 1 and 2 present how the progenitor number distribution of the merger tree realizations reproduces the theoretical prediction; $M_{\text{root}} = 1.3 \times 10^{11} M_{\odot}$ (*Left*) and $1.3 \times 10^{14} M_{\odot}$ (*Right*). In these plots, we adopt the logarithmically equal timestep in redshift:

$$z_{(i)} = (1 + z_{\text{min}}) \times \left(\frac{1 + z_{\text{max}}}{1 + z_{\text{min}}} \right)^{i/N_{\text{step}}} - 1 \quad (i = 1, \dots, N_{\text{step}}), \quad (6)$$

where N_{step} is the total number of the redshift bins. We defer the discussion of the choice of N_{step} to the next subsection (§ 2.3), and fix $N_{\text{step}} = 100$ throughout this subsection.

The top-panels in Figure 1 show the result for the 1st timestep ($i = 1$) corresponding to $z_{(1)} = 0.028$ according to equation (6). We call this model SK-n indicating the Somerville, Kolatt (1999) method with the number-weighted probability. The symbols indicate the average $(M_2/N_{\text{ens}})(\Delta N_2/\Delta M_2)$ with the quoted error-bars being the corresponding one-sigma dispersion, where ΔN_2 is the number of progenitors in the range of mass $M_2 \sim M_2 + \Delta M_2$, and we adopt $\Delta \log_{10} M_2 = 0.1$. In the SK-n model we generate the random numbers according to the number-weighted probability distribution function (eq.[5]). Also we have to set the lower limit on the progenitor mass in adopting the SK-n model so as avoid a divergent total probability. We adopted the lower limit of

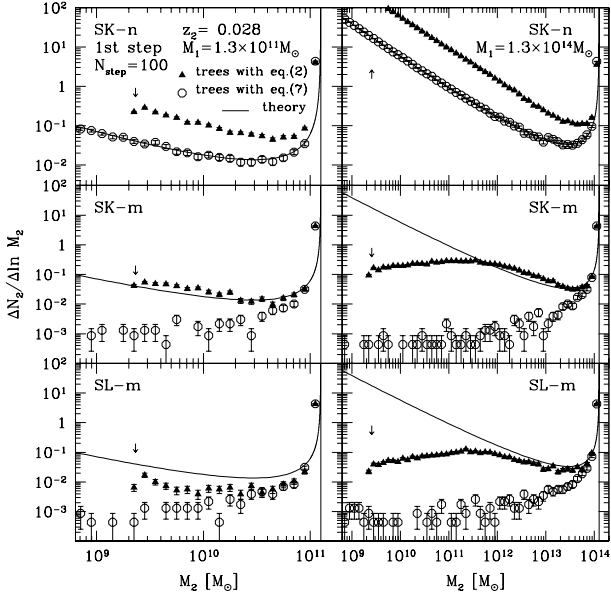


Fig. 1. Progenitor number distribution at the 1st timestep ($z_{(1)} = 0.028$ with $N_{\text{step}} = 100$ in eq.[6]) for $M_{\text{root}} = 1.3 \times 10^{11} M_{\odot}$ (Left) and $1.3 \times 10^{14} M_{\odot}$ (Right). Top (SK-n) and middle (SK-m) panels adopt the number-weighted and mass-weighted conditional progenitor probability functions (eqs.[5] and [4]) according to Somerville, Kolatt (1999), while bottom (SL-m) panels use the mass-weighted one according to Sheth, Lemson (1999). The theoretical prediction in the extended Press-Schechter theory (eq.[5]) is plotted in solid curves. The solid triangles and open circles indicate the averages over $N_{\text{ens}} = 10^4$ merging tree realizations with the different mass conservation prescriptions, eqs.(2) and (7), respectively. The quoted error bars represent the Poisson error in each mass bin, and the arrows indicate the value of M_{res} .

$10^{-3} M_{\text{res}}$, and made sure that the mass function of progenitors of the mass range of our interest $M > M_{\text{res}}$ is properly reproduced.

The solid triangles show our result based on the algorithm outlined in the previous subsection. Somewhat surprisingly, they are completely different from the theoretical distribution that we use in generating the trees (solid curve). Note that Figure 1 plots the number distribution multiplied by M_2 , $M_2 dN/dM_2 = M_1 dP/dM_2$ (see eq.[5]). To understand the origin of the discrepancy, we generate the progenitors at the 1st timestep for N_{ens} realizations simultaneously as long as they satisfy

$$\sum_{i=1}^{N'} M_2^i < N_{\text{ens}} [M_1 - \Delta M_{\text{acc}}(< M_{\text{res}})], \quad (7)$$

instead of the mass conservation (eq.[2]) for each individual parent halo. In the above, N' is not the number of progenitors for a single halo at $z = z_{\text{min}}$, but for an ensemble of N_{ens} halos with the same mass M_{root} . The resulting distribution is plotted in open circles, and in fact shows good agreement with the theoretical curve.

This is simply because we attempt to generate a joint distribution of progenitors with a repeated use of the conditional probability (eq.[5]) *incorrectly*; except for the first progenitor, the mass conservation for each halo (eq.[2])

introduces an additional cutoff at higher mass in the selection probability of progenitors. In fact the conditional probability (eq.[5]) for $(z_2 - z_1)/z_1 \ll 1$ is sharply peaked at a mass scale M_2 just below the parent mass M_1 , and thus even a small value of the first progenitor mass may effectively bias not to choose remaining progenitors in the peak. Thus the resulting distribution is significantly biased toward low mass objects, i.e., the number density of the low mass objects exceeds the theoretical predictions by an order of magnitude (top panels in Fig. 1).

A way out of this problem is to generate many (> 100) realizations simultaneously as Kauffmann, White (1993) adopted. Even in this case, one needs to specify an additional assumption on how to plant a set of progenitors in a single merger tree *by hand*. Moreover, a practical implementation of this method requires to discretize the halo mass and thus becomes computationally demanding as both the mass and time resolutions increase.

Another possibility is to artificially distort the input conditional probability so that the selected progenitors obey the distribution (eq.[5]). While the required correction may be a fairly definite mathematical problem, we do not know the exact answer, and thus have to proceed in a phenomenological fashion. Basically this is the approach taken by Somerville, Kolatt (1999) and Sheth, Lemson (1999), who adopted the *mass-weighted* probability (eq.[4]) as the theoretical input. The middle and bottom panels in Figure 1 show the resulting distribution for SK-m (Somerville, Kolatt 1999-mass weighted) and SL-m (Sheth, Lemson 1999-mass weighted), respectively. Clearly the resulting distributions (filled triangles) become much closer to equation (5) under the constraint (eq.[2]) although their original distributions (i.e., without the constraint [2]) plotted in open circles are completely different.

As this indicates, the input conditional probability for the current purpose should be small at lower mass scales of M_2 relative to equation (5). Thus we also attempted the probability proportional to $(M_1/M_2)^{\alpha} (dP/dM_2)$. Note that the mass- and number-weighted probabilities (eqs.[4] and [5]) correspond to $\alpha = 0$ and 1. We were not able to obtain a similar degree of agreement for a value of α very different from 0, but did not find a significant change for $-0.2 \lesssim \alpha \lesssim +0.2$. Thus we decided to adopt $\alpha = 0$ (the mass-weighted probability) as Somerville, Kolatt (1999). This choice has an advantage that a numerical routine to generate random numbers becomes easier than the cases of $\alpha \neq 0$. Define $x_2 = (\delta_{c,2} - \delta_{c,1})/\sqrt{S_2 - S_1}$ that obeys Gaussian distribution of a unit variance. Equation (4) implies that the desired distribution of M_2 can be simply given via $S_2 = S(M_2) = S_1 + (\delta_{c,2} - \delta_{c,1})^2/x_2^2$. Since the Gaussian distributed random numbers can be implemented easily, all we have to do is to supply the inverse function of the mass variance, $M_2 = S^{-1}(S_2)$. Our SK-m implementation seems to yield larger discrepancy between theory and the merger tree realizations at small M_2 regimes than their original results. This may be due to the different choice of the timestep and the condition how to stop selecting progenitor halos. In any case, however,

this discrepancy rapidly fades away in constructing the merger tree using many timesteps as we show in Figures 2 and 4.

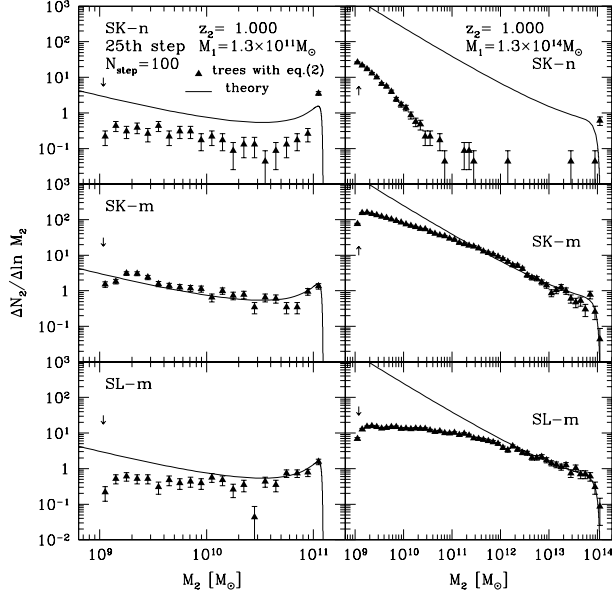


Fig. 2. The same as Fig. 1 except at the 25th timestep ($z_{(25)} = 0.028$) for the mass conservation prescription (eq.[2]); $M_{\text{root}} = 1.3 \times 10^{11} M_{\odot}$ (Left) and $1.3 \times 10^{14} M_{\odot}$ (Right).

Figure 2 plots the snapshot of the progenitor distribution at the 25th timestep ($z = z_{(25)} = 1.0$), which makes sure that the mass-weighted probability reasonably works even when we trace the merger tree by many steps. Also SK-m works a bit better than SL-m especially at small mass scales. Originally SL-m was proposed to correct for the halo exclusion effect, but does not work so efficiently at least in the range of parameters we surveyed. Figure 2 also indicates that SK-n is substantially different from the analytical solution. This is due to the fact that SK-n tends to select relatively less massive progenitors preferentially (see Fig.1), and this tendency simply accumulates in many steps. On the contrary, the behavior of SK-m and SL-m becomes closer to the analytical solution than in the case of Figure 1. This is because that the latter two models well approximate the probability distribution around M_1 which is the most important range when constructing the real merger trees with many timesteps.

2.3. Timestep

The next question that we address is the appropriate choice of the timestep. While this is an equally important problem in the Monte-Carlo modeling, the previous authors did not discuss it in an explicit manner.

Obviously the timestep needs to be smaller than the dynamical time-scale of halos just virialized at the redshift, $t_{\text{dyn,vir}}(z)$, because they are the objects that serve as the initial condition for the Monte-Carlo modeling. Figure 3 compares this time-scale and our choice (eq.[6]) for $N_{\text{step}} = 10, 100, 1000$. Also we plot the cosmic time $t_{\text{cosm}}(z)$ and the timestep corresponding to the linearly

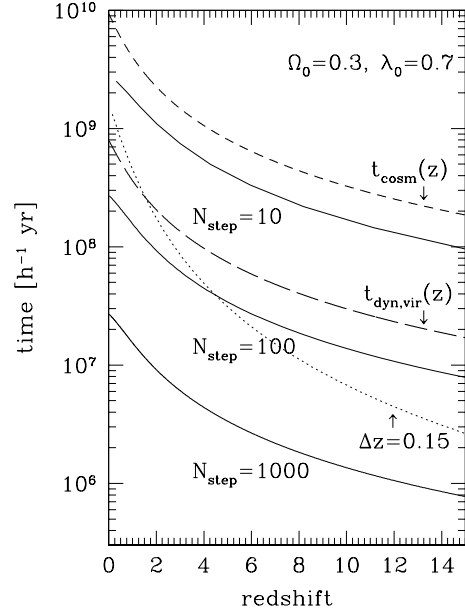


Fig. 3. Comparison among various timescales as a function of z in Λ CDM. Short-dashed and long-dashed curves indicate the cosmic time at z , and the dynamical time of dark halos just virialized at z . The dotted curve corresponds to the timesteps in linearly equal intervals in z , i.e., 100 bins between $z_{\text{min}} = 0$ and $z_{\text{max}} = 15$. Three solid curves correspond to the timesteps in logarithmically equal intervals in z ; $N_{\text{step}} = 10, 100$ and 1000 from top to bottom.

equal bin ($\Delta z = 0.15$). Even this simple comparison indicates that the logarithmic time bin with $N_{\text{step}} \gtrsim 100$ is required.

While the important question is how small timescales one should resolve, it critically depends on the problem that one would like to address. Therefore we rather ask with how many timesteps we can reproduce the progenitor distribution.

To see explicitly how different values of N_{step} affect the realizations of merger trees, we plot in Figure 4 the progenitor distribution with $N_{\text{step}} = 1000$ at redshift $z_{(1)} = 0.003$, $z_{(146)} = 0.499$, and $z_{(250)} = 1.0$. Comparison of Figures 2 and 4 indicates that the average progenitor distribution is indeed slightly better reproduced by $N_{\text{step}} = 1000$ than $N_{\text{step}} = 100$ particularly at small mass scales.

The difference between $N_{\text{step}} = 100$ and 1000 is more clearly illustrated when we plot the cumulative mass fraction of progenitors of mass exceeding a threshold value M_{thre} . More specifically, Figure 5 compares the theoretical prediction:

$$F_{\text{th}}(> M_{\text{thre}}; z) = \int_{M_{\text{thre}}}^{M_{\text{root}}} dM \frac{dP}{dM}(M, z | M_{\text{root}}, z_{\text{min}}), \quad (8)$$

with the average from the tree realizations:

$$F_{\text{model}}(> M_{\text{thre}}; z) = \frac{1}{N_{\text{ens}} M_{\text{root}}} \sum_{M_{\text{halo}}(z) \geq M_{\text{thre}}} M_{\text{halo}}(z) \quad (9)$$

for $M_{\text{root}} = 1.3 \times 10^{11} M_{\odot}$ (Left) and $1.3 \times 10^{14} M_{\odot}$ (Right).

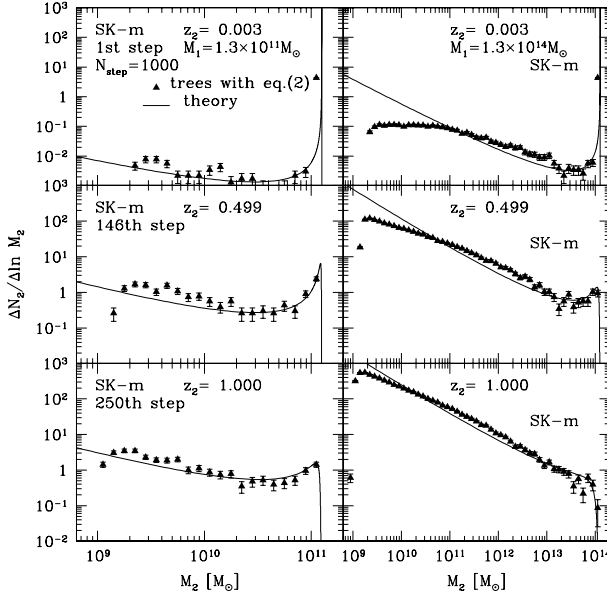


Fig. 4. Progenitor number distribution functions at the 1st, 146th and 250th steps from the $N_{\text{step}} = 1000$ merger trees using the SK-m method; $z_{(1)} = 0.003$ (Upper), $z_{(146)} = 0.499$ (Middle), and $z_{(250)} = 1.0$ (Lower). Left and right panels are for $M_{\text{root}} = 1.3 \times 10^{11} M_{\odot}$ and $1.3 \times 10^{14} M_{\odot}$. The theoretical prediction in the extended Press-Schechter theory (eq.[5]) is plotted in solid curves.

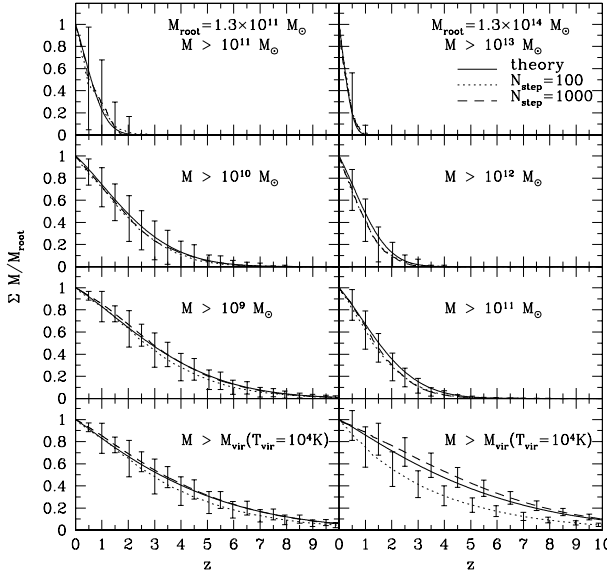


Fig. 5. Cumulative mass fraction of progenitors of mass exceeding a given threshold M_{thre} for $M_{\text{root}} = 1.3 \times 10^{11} M_{\odot}$ (Left) and $1.3 \times 10^{14} M_{\odot}$ (Right). The dotted and dashed curves indicate the averages from $N_{\text{step}} = 100$ and 1000 merger tree realizations with the corresponding Poisson error-bars.

In all panels shown here, the results with $N_{\text{step}} = 1000$ better reproduce the theoretical prediction mainly because of the small scale behavior (see Figs. 2 and 4). Since these small mass progenitors at earlier redshifts significantly contribute to radiative cooling and thereby subsequent star formation in the entire halo, this difference is

indeed critical in the Monte-Carlo modeling of galaxy formation. We will discuss the effect on gas cooling explicitly in the next section.

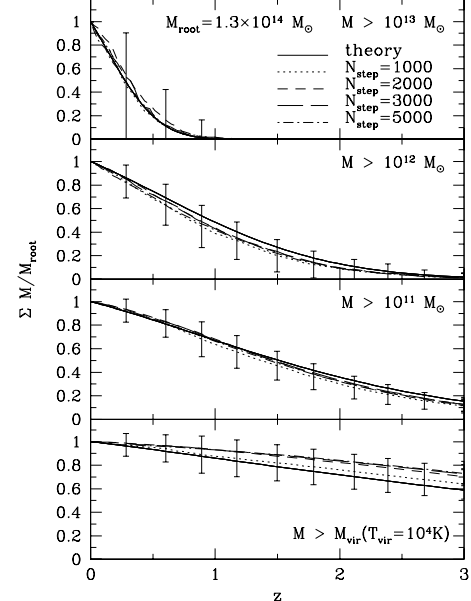


Fig. 6. Cumulative mass fraction of progenitors with different values of N_{step} for $M_{\text{root}} = 1.3 \times 10^{14} M_{\odot}$.

We interpret the above as an empirical result due to the balance between the mass-weighted probability and the timesteps. If the use of the mass-weighted probability were strictly justified, the proper realizations with smaller timestep would become more difficult numerically, and there is no reason why we could obtain better agreement with larger N_{step} . On the other hand, we understand that the mass-weighted probability is nothing but a phenomenological remedy of the problem, and with this choice $N_{\text{step}} = 1000$ seems to work better than $N_{\text{step}} = 100$ empirically.

In fact, still larger values of N_{step} do not necessarily improve the result. Figure 6 is a similar plot as Figure 5 for $M_{\text{root}} = 1.3 \times 10^{14} M_{\odot}$ but with increasing N_{step} . The cumulative mass fraction for $M > 10^{11} M_{\odot}$ is almost unchanged, but the contribution from smaller mass progenitors steadily increases as N_{step} becomes larger. This reflects the fact that the empirical use of the mass-weighted conditional probability does not guarantee the convergence of the result with respect to N_{step} .

Thus we conclude that $N_{\text{step}} \sim 1000$ is an optimal value to reproduce the Press-Schechter mass function in our method.

2.4. Number of progenitors

Finally we briefly discuss how many progenitors, N_{prog} , one should keep in order to properly reproduce the merger trees. Figure 7 displays the distribution functions at $z = 1$ for the merger tree of $M_{\text{root}} = 1.3 \times 10^{14} M_{\odot}$ at $z = 0$. In this particular example, we use $N_{\text{step}} = 1000$ and the results are averaged over $N_{\text{ens}} = 100$ realizations for each

N_{prog} . Obviously a smaller value of N_{prog} does not properly link the merger tree back to higher redshifts, and the number of small-mass halos is systematically underpredicted compared with the extended Press-Schechter model (solid curve). While we do not set any upper limit on N_{prog} , Figure 7 indicates that $N_{\text{prog}} \gtrsim 5$ is acceptable given the accuracy of the present scheme. Although some authors employ a binary merger tree in the Monte-Carlo modeling, that scheme needs to be adjusted with a careful choice of the timestep and other parameters.

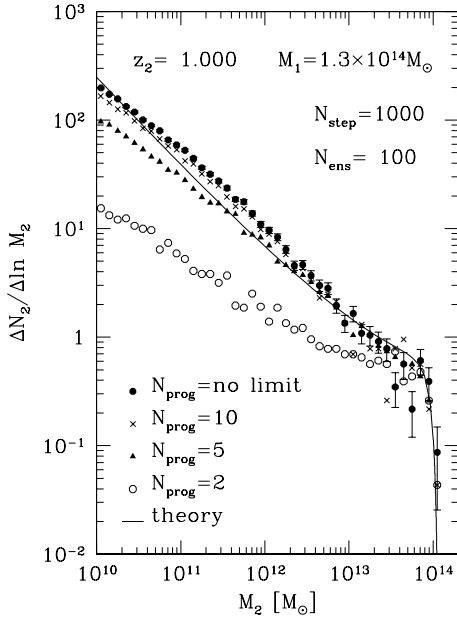


Fig. 7. The effect of the upper limit on the number of progenitors, N_{prog} , on the progenitor distribution function for $M_{\text{root}} = 1.3 \times 10^{14} M_{\odot}$ at $z = 1.0$ from $N_{\text{ens}} = 100$ merger tree realizations with $N_{\text{step}} = 1000$. The solid line is the number-weighted probability function, eq.(5). Filled circles indicate results with all progenitors satisfying the mass conservation (eq.[2]), while crosses, filled triangles, and open circles are for $N_{\text{prog}} = 10$, 5 and 2, respectively.

In conclusion, we have found a reasonable agreement between the theory and the merger tree realizations can be obtained by employing the mass-weighted conditional probability into the Somerville, Kolatt (1999) scheme with $N_{\text{step}} \sim 1000$.

3. Gas cooling

So far we have restricted our discussion to the gravitational aspect of the halo evolution. We next consider how the resulting merger trees affect the cold gas fraction in an individual halo. Of course we have to eventually discuss the effects on the efficiency of star formation, but we focus on gas cooling alone since modeling star formation, the feedback from supernovae, the chemical evolution and so on necessarily introduce additional (numerical) parameters and the interpretation becomes more complicated. Thus the principal aim of this section is to see if we can achieve a convergence of the cold gas fraction from the

different realizations of the merger trees.

3.1. Description of gas cooling

Our prescription of gas cooling in the merger trees goes as follows. First we assume that the density profile of dark halos obeys the universal shape (Navarro et al. 1996):

$$\rho_{\text{halo}}(r; M) = \begin{cases} \frac{\bar{\rho}(z) \delta_c}{(r/r_s)(1+r/r_s)^2} & (r < r_{\text{vir}}) \\ 0 & (r > r_{\text{vir}}) \end{cases}, \quad (10)$$

where $\bar{\rho}(z) \equiv \Omega_0 \rho_{\text{c}0} (1+z)^3$ is the mean density of the universe at z , $\rho_{\text{c}0}$ is the present critical density, $\delta_c(M)$ is the characteristic density excess, and $r_{\text{vir}}(M)$ and $r_s(M)$ indicate the virial radius and the scale radius of the halo, respectively.

The virial radius is defined according to the spherical collapse model as

$$r_{\text{vir}}(M) \equiv \frac{3M}{4\pi\bar{\rho}\Delta_{\text{nl}}}, \quad (11)$$

and the useful approximations for the critical over-density $\Delta_{\text{nl}} = \Delta_{\text{nl}}(\Omega_0, \lambda_0)$ may be found in Kitayama, Suto (1996). The two parameters r_s and r_{vir} are related in terms of the concentration parameter:

$$c(M, z) \equiv \frac{r_{\text{vir}}(M, z)}{r_s(M, z)}. \quad (12)$$

We use the approximate fitting function from the simulation data of Bullock et al. (2001):

$$c(M, z) = \frac{8.0}{1+z} \left(\frac{M}{10^{14} M_{\odot}} \right)^{-0.13}. \quad (13)$$

The condition that the total mass inside r_{vir} is equal to M relates δ_c to c as

$$\delta_c = \frac{\Delta_{\text{nl}}}{3} \frac{c^3}{\ln(1+c) - c/(1+c)}. \quad (14)$$

Makino et al. (1997) showed that if the hot gas is isothermal and in hydrostatic equilibrium, the gas density profile is well approximated by the isothermal β -model:

$$\rho_{\text{hot}}(r) = \frac{\rho_{\text{hot},0}}{[1 + (r/r_c)^2]^{3\beta/2}}, \quad (15)$$

where $r_c \sim 0.22r_s$. We fix $\beta = 2/3$ for simplicity. The amplitude $\rho_{\text{hot},0}$ is computed so as to reproduce the total hot gas in the halo when integrated up to $r = r_{\text{vir}}$. The hot gas is gradually converted to cold gas according to the prescription below, but still the total baryon (hot + cold) fraction within the virial radius of each halo is set to the cosmic average, Ω_B/Ω_0 .

Once the gas profile is specified, one can compute the cooling timescale at a radius r from the center of the halo:

$$t_{\text{cool}} = \frac{3}{2} \frac{\rho_{\text{hot}}(r)}{\mu m_p} \frac{k_B T_{\text{gas}}}{\Lambda(T_{\text{gas}}) n_{\text{H}}^2(r)}, \quad (16)$$

where μ is the mean molecular weight, m_p is the proton mass, k_B is the Boltzmann constant, $\Lambda(T_{\text{gas}})$ is radiative cooling function for gas of temperature T_{gas} , and $n_{\text{H}}(r)$ is number density of hydrogen (including both neutral and

ionized). We assume that the gas has the primordial abundance of hydrogen and helium ($X = 0.76$ and $Y = 0.24$, and thus $n_{\text{H}} = \rho_{\text{hot}}/Xm_{\text{p}}$), and compute the corresponding cooling function $\Lambda(T)$ (e.g., Sasaki, Takahara 1994). Since we neglect the molecular and metal cooling, $\Lambda(T) = 0$ at $T \leq 10^4$ K.

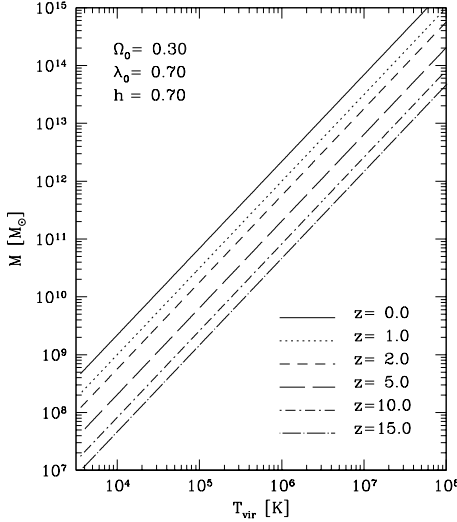


Fig. 8. Mass of halos as a function of the virial temperature at different redshifts in the Λ CDM model.

We further assume that the temperature of the hot gas, T_{gas} , is equal to the virial temperature, T_{vir} , of the halo. The relation between the virial temperature and the mass of a halo is plotted in Figure 8. Then we can solve equation (16) for the cooling radius, r_{cool} , within which the gas can cool within a given cooling timescale τ_{cool} :

$$r_{\text{cool}}(\tau_{\text{cool}}) \equiv 0.22 \frac{r_{\text{vir}}(M, z)}{c(M, z)} \sqrt{\frac{2\mu\Lambda(T_{\text{vir}})\rho_{\text{hot},0}\tau_{\text{cool}}}{3m_{\text{p}}k_{\text{B}}T_{\text{vir}}}} - 1. \quad (17)$$

It now remains to define the origin of τ_{cool} . Actually this is fairly arbitrary in a sense, and we adopt the following simple picture. When a halo of mass M_f forms at the formation redshift z_f , its hot gas is supposed to reach the profile (eq.[15]) instantaneously. This is defined to be the origin of τ_{cool} for the halo. In the subsequent timesteps, we neglect the change in the hot gas profile even if the halo mass M grows due to mergers and the cooling radius is computed with τ_{cool} set to the elapsed cosmic time since z_f . When M exceeds $2M_f$, the halo is replaced by a *newly* formed massive halo, and the hot gas profile is reset to the profile (eq.[15]) corresponding to the new mass and the virial temperature, and we reset the origin of τ_{cool} as the new formation epoch. Incidentally we made sure that the value of $1.5M_f$ instead of $2M_f$ does not change the result which is consistent with the finding of Cole et al. (2000). We apply this procedure for all halos, and the cold gas in each progenitor halo is simply accumulated (without reheated) according to the merger trees.

3.2. Cold gas fraction in the Monte-Carlo realization of merging histories

In a practical implementation of the merger tree algorithm, one has to stop tracing the progenitors of halos of mass below the resolution mass M_{res} . We discuss the relevance of our choice of M_{res} by looking at the cold gas fraction. Previous authors often apply the cutoff at a fixed mass or a circular velocity of halos; for instance, Cole et al. (2000) consider halos with $M > 5 \times 10^9 h^{-1} M_{\odot}$ in their merger trees while Somerville, Primack (1999) take account of halos with the circular velocity exceeding 40 km/s (corresponding to the virial temperature $T_{\text{vir}} \sim 6 \times 10^4$ K). The latter condition comes from an estimate of the smallest scale of halos which can cool in the presence of the UV background (e.g., Thoul, Weinberg 1996; Kitayama, Ikeuchi 2000).

In our present analysis, the cooling function $\Lambda(T)$ vanishes below $T = 10^4$ K since we neglect both UV heating and metal/molecular cooling. Thus we set the resolution mass $M_{\text{res}}(z)$ as $M(T_{\text{vir}} = 10^4$ K). As Figure 8 shows, this scale increases rapidly with time and resulting in a significant improvement of the computing time. On the other hand, this might systematically underestimate the cold gas fraction since halos of mass below $M_{\text{res}}(z_1)$ may have progenitors of mass larger than $M_{\text{res}}(z_2)$ at the earlier epoch ($z_2 > z_1$). Fortunately this is not an important effect as we show below.

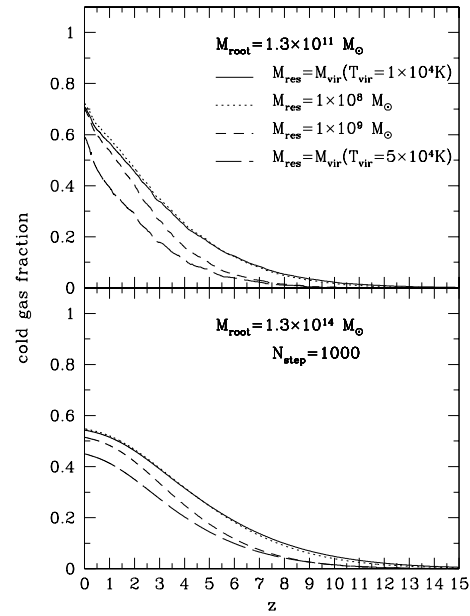


Fig. 9. Cold gas fraction (eq.[18]) with different resolution mass M_{res} averaged from $N_{\text{ens}} = 10$ merging tree realizations at $N_{\text{step}} = 1000$. Upper and lower panels show the results for $M_{\text{root}} = 1.3 \times 10^{11} M_{\odot}$ and $1.3 \times 10^{14} M_{\odot}$; $M_{\text{res}}(z) = M(T_{\text{vir}} = 10^4 \text{ K})$, $M(T_{\text{vir}} = 5 \times 10^4 \text{ K})$, $10^8 M_{\odot}$, and $10^9 M_{\odot}$.

To see this in detail, we plot in Figure 9 the cold gas fraction averaged over all progenitors at z of a root halo of mass M_{root} at $z = 0$:

$$f_{\text{cold}}(z; M_{\text{root}}) \equiv \frac{\Omega_0}{\Omega_B M_{\text{root}}} \sum_{M_{\text{prog}} > M_{\text{res}}} M_{\text{cold}}(M_{\text{prog}}), \quad (18)$$

for a merger tree with $N_{\text{step}} = 1000$. If we adopt a constant value for the resolution mass, $M_{\text{res}} < 10^8 M_{\odot}$ yields the convergent result for the cold gas fraction. Exactly the same convergence is obtained for the time-dependent $M_{\text{res}}(z)$ when the value is set to $M(T_{\text{vir}} = 10^4 \text{ K})$, but not if we use $M(T_{\text{vir}} = 5 \times 10^4 \text{ K})$, for instance. This critical value is expected to vary depending on the thermal history of the universe, but the appropriate value for T_{vir} is straightforwardly read off from the relevant cooling function. Actually $M_{\text{res}}(z)$ increases in this case and exceeds $10^9 M_{\odot}$ (see Fig. 8). Thus the required merging tree is less demanding from the computational point of view than that for $M_{\text{res}} = 10^8 M_{\odot}$, for instance, as illustrated in Table 2. Thus we decide to choose $M_{\text{res}}(z) = M(T_{\text{vir}} = 10^4 \text{ K})$ for gas with the primordial abundance.

Finally we show the convergence with respect to N_{step} . Figure 10 plots the cold gas fraction for $M_{\text{root}} = 1.3 \times 10^{11} M_{\odot}$ (*Upper*) and $1.3 \times 10^{14} M_{\odot}$ (*Lower*) for merging trees with different N_{step} . The results are fairly in agreement for small M_{root} , but are very different for large M_{root} . This is because the merger tree at small mass scales, especially at $M(T_{\text{vir}} = 10^4 \text{ K}) < M < 10^{10} M_{\odot}$, is well reproduced only when we use $N_{\text{step}} = 1000$ (see Fig. 5). When we repeat the same calculation sampling every 10 steps from the $N_{\text{step}} = 1000$ tree, the result is almost indistinguishable. Thus we conclude that the progenitor distribution at small scales is quite essential in the estimate of the cold mass fraction of large halos.

Incidentally the use of the timestep much smaller than $t_{\text{dyn,vir}}(z)$ enables one to describe the collapse and gas cooling more realistically than the instantaneous approximation. While we do not attempt this in the present paper, this would improve the estimate of the cold gas fraction quantitatively.

4. Conclusions and Discussion

We attempted several convergence tests of the merger trees generated with the Monte-Carlo method. While this method provides a useful tool of modeling galaxy formation in a complementary manner to more intensive cosmological simulations with ad hoc recipes of galaxy formation (e.g., Cen, Ostriker 1992; Weinberg et al. 1997; Yoshikawa et al. 2001), the lack of the explicit expression for the joint distribution function of progenitors (eq.[1]) requires one to put an additional assumption in practice. We confirmed that a repeated use of the *mass-weighted* conditional probability (eq.[5]) reasonably reproduces the progenitor distribution predicted in the extended Press-Schechter theory if one adopts fairly small timesteps in redshift, $N_{\text{step}} \sim 1000$, a factor of ten larger than a typical value used in previous work. We note, however, that one can alternatively achieve the similar result by fine-tuning the timestep as a function of M_1 (e.g., Somerville, Kolatt 1999) instead of equation (6) as we adopted here.

One may avoid the above problem also by using merger

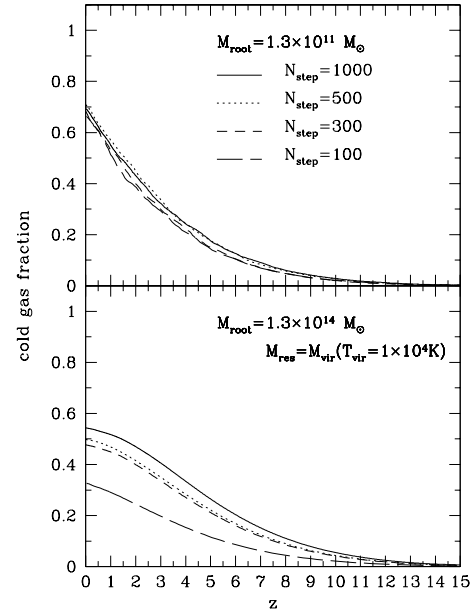


Fig. 10. Cold gas fraction averaged from $N_{\text{ens}} = 10$ merger tree realizations with different N_{step} . Upper and lower panels show the results for $M_{\text{root}} = 1.3 \times 10^{11} M_{\odot}$ and $1.3 \times 10^{14} M_{\odot}$. The resolution mass of the tree is fixed as $M_{\text{res}}(z) = M(T_{\text{vir}} = 10^4 \text{ K})$.

trees generated via N-body simulations (Kauffmann et al. 1999; Somerville et al. 2001). In fact they claim that the agreement between the N-body simulations and the Monte-Carlo method is good. Benson et al. (2001) compared the SPH simulations and the Monte-Carlo modeling, and concluded that both agree with each other on the cold gas mass fraction and mass function of the halos. While this comparison is encouraging, it is not yet clear if the lack of the joint distribution function of progenitors (eq.[1]) in the Monte-Carlo modeling may not be essential. Thus further detailed studies are definitely important to test the reliability of *both* N-body and the Monte-Carlo modeling in generating merger tree realizations.

We thank Kazuhiro Shimasaku and Tomonori Totani for discussions and suggestions in the early phase of this work. This research was supported in part by the Grant-in-Aid from Monbu-Kagakusho, Japan (07CE2002, 12304009, 12640231). T.K. gratefully acknowledges support from Research Fellowships of the Japan Society for the Promotion of Science for Young Scientists (7202).

References

Arimoto, N., & Yoshii, Y. 1986, A&A, 164, 260

Baugh, C. M., Cole, S., Frenk, C. S., & Lacey, C. G. 1998, ApJ, 498, 504

Benson, A. J., Pearce, F. R., Frenk, C. S., Baugh, C. M., & Jenkins, A., 2001, MNRAS, 320, 261

Bond, J., Cole, S., Efstathiou, G., & Kaiser, N. 1991, ApJ, 379, 440

Bower, R. 1991, MNRAS, 248, 332

Bruzual A., G. 1983, ApJ, 273, 105

Bruzual A., G., & Charlot, S. 1993, ApJ, 405, 538

Bullock, J. S., Kolatt, T. S., Sigad, Y., Somerville, R. S., Kravtsov, A. V., Klypin, A. A., Primack, J. R., & Dekel, A. 2001, MNRAS, 321, 559

Charlot, S., & Bruzual A., G. 1991, ApJ, 367, 126

Cen, R. Y., & Ostriker, J. P. 1992, ApJ, 399, L113

Cole, S. 1991, ApJ, 367, 45

Cole, S., Aragón-Salamanca, A., Frenk, C., Navarro, & J., Zepf, S. 1994, MNRAS, 271, 781

Cole, S., & Kaiser, N. 1988, MNRAS, 233, 637

Cole, S., Lacey, C. G., Baugh, C. M., & Frenk, C. S. 2000, MNRAS, 319, 168

Guiderdoni, B., & Rocca-Volmerange, B. 1987, A&A, 186, 1

Kauffmann, G., & White, S. 1993, MNRAS, 261, 921

Kauffmann, G., White, S., & Guiderdoni, B. 1993, MNRAS, 264, 201

Kauffmann, G., Colberg, J. M., Diaferio, A., & White, S. D. M. 1999, MNRAS, 303, 188

Kitayama, T., & Ikeuchi, S. 2000, ApJ, 529, 615

Kitayama, T., & Suto, Y. 1996, ApJ, 469, 480

Kitayama, T., & Suto, Y. 1997, ApJ, 490, 557

Kitayama, T., Sasaki, S., & Suto, Y. 1998, PASJ, 50, 1

Kodama, T., & Arimoto, N. 1997, A&A, 320, 41

Lacey, C., & Cole, S. 1993, MNRAS, 262, 627

Makino, N., Sasaki, S., & Suto, Y. 1997, ApJ, 497, 555

Nagashima, M., & Gouda, N. 2001, MNRAS, 325, L13

Navarro, J. F., Frenk, C. S., & White, S. D. M. 1996, ApJ, 462, 563

Sasaki, S., & Takahara, F. 1994, Prog. Theor. Phys., 91, 699

Sheth, R. K., & Lemson, G. 1999, MNRAS, 305, 946

Somerville, R. S., & Kolatt, T. S. 1999, MNRAS, 305, 1

Somerville, R., & Primack, J. 1999, MNRAS, 310, 1087

Somerville, R. S., Lemson, G., Sigad, Y., Dekel, A., Kauffmann, G., & White, S. D. M. 2001, MNRAS, 320, 289

Tinsley, B. M. 1980, ApJ, 241, 41

Thoul, A. A., & Weinberg, D. H., 1996, ApJ, 465, 608

Weinberg, D. H., Hernquist, L., & Katz, N. 1997, ApJ, 477, 8

White, S., & Frenk, C. 1991, ApJ, 379, 52

Yoshikawa, K., Taruya, A., Jing, Y. P., & Suto, Y. 2001, ApJ, 558, 520

Table 1. Summary of variables used in building merger trees and in gas cooling.

symbol	adopted value	physical meaning
M_{root}	—	mass of halo at $z = z_{\text{min}}$
T_{vir}	—	virial temperature of halo
M_{res}	$M(T_{\text{vir}} = 10^4 \text{ K})$	minimal mass of progenitors resolved in each merger tree
τ_{cool}	halo mass doubling time	cooling time scale for gas in hosting halos
N_{step}	1000	number of redshift bins (logarithmically equal interval)
N_{ens}	—	number of realizations of merger trees
z_{min}	0	minimum redshift of merger trees
z_{max}	15	maximum redshift of merger trees

Table 2. CPU timing of the Monte-Carlo modeling for one merger tree on a 21264 alpha 600 MHz machine.

M_{root}	N_{step}	M_{res}	# of progenitors	CPU-time	
				merger tree	gas cooling
$1.3 \times 10^{11} M_{\odot}$	100	$10^8 M_{\odot}$	3876	3.4 sec	0.55 sec
$1.3 \times 10^{11} M_{\odot}$	100	$M(T_{\text{vir}} = 10^4 \text{ K})$	1687	2.9 sec	0.43 sec
$1.3 \times 10^{11} M_{\odot}$	1000	$10^8 M_{\odot}$	56057	15.1 sec	4.4 sec
$1.3 \times 10^{11} M_{\odot}$	1000	$M(T_{\text{vir}} = 10^4 \text{ K})$	20556	6.8 sec	2.3 sec
$1.3 \times 10^{14} M_{\odot}$	100	$10^8 M_{\odot}$	1122420	244 sec	75.6 sec
$1.3 \times 10^{14} M_{\odot}$	100	$M(T_{\text{vir}} = 10^4 \text{ K})$	640409	137 sec	46.5 sec
$1.3 \times 10^{14} M_{\odot}$	1000	$10^8 M_{\odot}$	29725672	6514 sec	1993 sec
$1.3 \times 10^{14} M_{\odot}$	1000	$M(T_{\text{vir}} = 10^4 \text{ K})$	18875982	4140 sec	1400 sec